Multilayer Formulation of the Fragment Molecular Orbital Method (FMO)

Dmitri G. Fedorov,* Toyokazu Ishida, and Kazuo Kitaura

National Institute of Advanced Science and Technology (AIST), Umezono, Tsukuba, Ibaraki, Japan 305-6568

Received: June 28, 2004; In Final Form: November 30, 2004

The fragment molecular orbital method (FMO) has been generalized to allow for multilayer structure. Fragments are assigned to layers, and each layer can be described with a different basis set and/or level of electron correlation. Interlayer boundaries are treated in the general spirit of the FMO method since they also coincide with some interfragment boundaries. The question of the one- and two-layer FMO accuracy dependence upon the fragmentation scheme is also addressed. The new method has been applied to predict the reaction barrier and the reaction heat for the Diels−Alder reaction with a representative set of reactants based on dividing fragments in two layers. The 6-31G* basis set has been used for the active site and the 6-31G*, 6-31G, 3-21G, and STO-3G basis sets have been used for the substituents. Different levels of electron correlation (RHF, B3LYP, and MP2) have been applied to layers in systematic fashion. The one-layer FMO errors in the reaction barrier and the reaction heat were 2.0 kcal/mol or less for all levels applied (RHF, B3LYP, and MP2), relative to full ab initio methods. For the two-layer method the error was found to be several kcal/mol. Benchmark calculations of the activation barrier for the decarboxylation of phenylcyanoacetate by β-cyclodextrin demonstrated that the two-layer calculations are efficient, being 36 times faster than the regular DFT, as well as accurate, with the error being 1.0 kcal/mol.

1. Introduction

Large biological molecules present a serious challenge to computational quantum chemistry. General ab initio-based methods, while potentially having sufficient accuracy, become too expensive as the number of atoms grows to hundreds or thousands, depending on the calculation level. The fragment molecular orbital (FMO) method originally proposed by Kitaura et al.[1] very closely resembles fully ab initio methods. By dividing molecules into fragments and performing monomer, dimer, and optionally trimer ab initio calculations of fragments and combining the obtained results, one can very closely reproduce the full ab initio properties, such as total energies, gradients, and dipole moments.

Nearly analytic gradients have been developed by Kitaura et al.,[2] and the FMO method has become computationally feasible with the development of approximations by Nakano et al.[3] The method has been combined with molecular dynamics by Komeiji et al.,[4] and the recent comprehensive study by Fedorov and Kitaura[5] confirmed high accuracy of the two- and three-body FMO method on a range of representative molecules based on the restricted Hartree−Fock (RHF) theory. The importance of the electron correlation for practical applications prompted the development of the density functional theory (DFT)-based FMO method (FMO-DFT[6]), the second-order Møller−Plesset (MP2)-based FMO method (FMO-MP2[7]), and the multiconfiguration self-consistent field (MCSCF)-based FMO (FMO-MCSCF[8]).

The first subject addressed in this work encompasses accuracy tests elucidating bond fractioning in the FMO method. Several ways to perform fragmentation of molecules are attempted, and the obtained results are analyzed in terms of their performance. Second, we apply the FMO method to the very important and widely studied Diels−Alder reaction in order to estimate the accuracy and validity of the FMO method applied to chemical

reactions. To the best of our knowledge, this is the first application of the FMO method to activation barriers and reaction heats. Third, we present multilayer FMO method that allows combining several basis sets and/or electron correlation levels in a single calculation, aimed at a further increase in computational efficiency. It is quite common that one is able to select the most important (active) part of a molecule that has to be described most accurately, whereas the remaining parts can be treated with computationally cheaper methods. Several other approaches sharing this idea have been proposed, in particular, the ONIOM method by Svensson et al.[9] In this work we present the multilayer FMO method based on single reference wave functions. The multireference version of the multilayer FMO method is presented elsewhere.[8]

The main distinction between the multilayer FMO method and the other approaches similar in spirit is the absence of hydrogen caps, which permits proper physical description of the boundaries between layers while retaining high accuracy attested to the FMO method by previous studies.[5] Second, in the FMO method at all stages the full system is present and exerts its influence through rigorous Coulomb field, whereas in other schemes[9] one relies on additivity of extrapolation schemes that may or may not work, depending on how different electron density distribution is in various size models therein. By using multilayer structure, one replaces a higher level description of fragment electron densities with a computationally cheaper one while treating electron correlation at lower levels for less important regions of the system. We note in passing that the multilayer FMO method provides quantitative interfragment interaction details similar to the unilayer method.

Two-layer two-body FMO studies of the Diels−Alder reaction are conducted, mixing separately basis sets and wave function (RHF, DFT, and MP2) types, as well as mixing both basis sets and wave function types in the same calculation. The basis sets were chosen to be those practically usable in real

---

Multilayer Fragment Molecular Orbital Method

J. Phys. Chem. A, Vol. 109, No. 11, 2005 **2639**
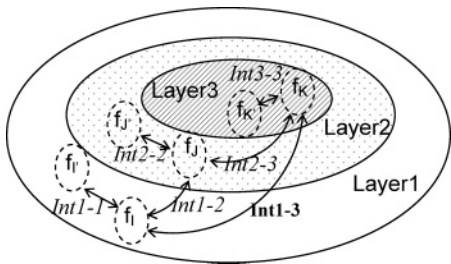
Figure 1. An example of the three-layer FMO2 method. All fragments (denoted by *f*) are divided into three layers. Pair interactions (Int*i-j*) within each layer $i = j$ are computed using wave function and the basis set corresponding to this layer. Interlayer pair interactions for $i \neq j$ are computed at the lower level (corresponding to the lower layer $k = \min(i,j)$).

applications of the method to very large biological molecules. The Diels−Alder reaction has been extensively studied previously[10,11] and it represents an appropriate test case where electron correlation plays an important role and proper description of substituents is necessary. The main purpose of the calculations in this work is to demonstrate the efficiency of the multilayer approach that permits significant cost reduction while keeping sufficient accuracy. The goal is to reproduce high level properties (e.g., FMO2-MP2/6-31G* for the whole system) by treating only the active (reaction) site with an expensive method (e.g., MP2/6-31G*) and the rest at a cheaper level (e.g., RHF/3-21G). Finally, some benchmarking calculations are performed demonstrating both accuracy and computational efficiency of the multilayer approach.

2. Methodology

The original formulation of the FMO method[5] is based on the following equation:

$$E = \sum_I^N E_I + \sum_{I>J}^N (E_{IJ} - E_I - E_J) + \sum_{I>J>K}^N \{(E_{IJK} - E_I - E_J - E_K) - (E_{IJ} - E_I - E_J) - (E_{JK} - E_J - E_K) - (E_{KI} - E_K - E_I)\} + \cdots \quad (1)$$

Monomer (E_I), dimer (E_{IJ}), and trimer (E_{IJK}) energies are obtained from corresponding single-point *n*-mer calculations ($n = 1,2,3$) in the external filed due to remaining monomers, performed at the appropriate level of electron correlation, and *N* is the number of fragments.

In the multilayer method, all fragments are divided into layers. For each layer, a separate level of electron correlation and/or basis set can be specified. Higher layers correspond to larger basis sets and/or higher levels of electron correlation. An example of layer division is illustrated in Figure 1 for the case of three layers. The layer structure should not be taken geometrically; that is, one can put remote parts of the system in the same layer if desired. For notation we generalize the previously suggested one[5] and list electron correlation levels and basis sets in ascending order of layers, separated by semicolons, e.g., FMO2−RHF/3-21G:MP2/6-31G* means the two-layer two-body FMO method with layer 1 described by RHF and the 3-21G basis set, and layer 2 described by MP2 and the 6-31G* basis set. For a short-hand notation, if the basis sets are the same or otherwise indicated or understood we write FMO2−RHF:MP2. In this work we use the same *n*-body expansion for all layers. Should in the future a need arise to assign a different many-body expansion per layer, the notation may look like FMO3−RHF:FMO2-MP2 if three-body expansion is desired for layer 1 and two-body for layer 2.

The multilayer FMO method is based on the following equation:

$$E = \sum_I^N E_I^{L_I} + \sum_{I>J}^N (E_{IJ}^{L_{IJ}} - E_I^{L_{IJ}} - E_J^{L_{IJ}}) + \sum_{I>J>K}^N \{(E_{IJK}^{L_{IJK}} - E_I^{L_{IJK}} - E_J^{L_{IJK}} - E_K^{L_{IJK}}) - (E_{IJ}^{L_{IJK}} - E_I^{L_{IJK}} - E_J^{L_{IJK}}) - (E_{JK}^{L_{IJK}} - E_J^{L_{IJK}} - E_K^{L_{IJK}}) - (E_{KI}^{L_{IJK}} - E_K^{L_{IJK}} - E_I^{L_{IJK}})\} + \dots \quad (2)$$

where L_I denotes the layer to which fragment *I* belongs; $L_{IJ} = \min(L_I,L_J)$ and $L_{IJK} = \min(L_I,L_J,L_K)$. Monomer ($E_I^{L_1}$), dimer ($E_{IJ}^{L_2}$), and trimer ($E_{IJK}^{L_3}$) energies are obtained for corresponding *n*-mers ($n = 1,2,3$) at the level defined by layers L_1, L_2, and L_3, respectively. Equation 2 reduces to eq 1 for the case of one layer. It can be seen from eq 2 that monomer energies E_I enter at the level L_I, whereas pair and higher order *n*-body corrections enter at the lowest level of all monomers making the corresponding *n*-mer. Boundaries between layers (that are also boundaries between fragments) are handled in the same way as boundaries between fragments in the single layer FMO method,[5] the only difference being the use of projection operators based on the basis set for the given layer. In other words, no hydrogen caps are used and the bonds are fractioned electrostatically, as in the single-layer case.

The external electrostatic potentials (ESP) used during the computation of E_x^L ($x = I$, *IJ*, or *IJK*) is computed for the given layer *L* as follows (compare to ref 5):

$$V_{\mu\nu}^{x(L)} = \sum_{K \neq x} \left\{ \sum_{A \in K} \left\langle \mu \left| -\frac{Z_A}{|\mathbf{r} - \mathbf{R}_A|} \right| \nu \right\rangle + \sum_{\rho\sigma \in K} D_{\rho\sigma}^{K(\tilde{L}_K)} (\mu\nu|\rho\sigma) \right\} \quad (3)$$

where $D^{K(\tilde{L}_K)}$ denotes electron density of fragment *K* computed in the layer $\tilde{L}_K = \min(L_K,L)$. Projection operators[5] added to the Fock matrix are computed with the basis set specific for the given layer. With the exception of using energies, electron densities, and projection operators for the appropriate layer, unilayer and multilayer formulations of the FMO method are the same.

The computational scheme for the multilayer FMO method is given in Figure 2. Equation 2 can be rewritten in order to better demonstrate the actual implementation:

$$E = \sum_{i=1}^M \{ \sum_{I \in i}^N (E_I^i + \sum_{j=i}^M \sum_{\substack{J=1, \\ J \in j}}^{I-1} [(E_{IJ}^i - E_I^i - E_J^i) + \sum_{\substack{K=1, \\ K \in j}}^{J-1} \{(E_{IJK}^i - E_I^i - E_J^i - E_K^i) - (E_{IJ}^i - E_I^i - E_J^i) - (E_{JK}^i - E_J^i - E_K^i) - (E_{KI}^i - E_K^i - E_I^i)\} + \dots])\} \quad (4)$$

where *i* runs through *M* layers.

The calculation begins with layer 1 and exactly follows the single-layer FMO method formalism, except that only those dimers *IJ*, trimers *IJK*, and, if needed, correlated monomers *I* are computed, for which *I* belongs to layer 1 (i.e., $L_I = 1$). Next, layer 2 calculations begin with generating initial orbitals for all fragments that belong to layers 2 or higher, followed by monomer SCF iterations for these monomers. ESPs due to fragments in layer 1 are computed using electron densities for the corresponding monomers obtained during layer 1 calculations, following eq 3. Next, dimers *IJ*, trimers *IJK* and, if needed, correlated monomers *I* are computed, for which (a) *I* belongs to layer 2 and (b) *J* (in dimers) or *J,K* (in trimers) belong to
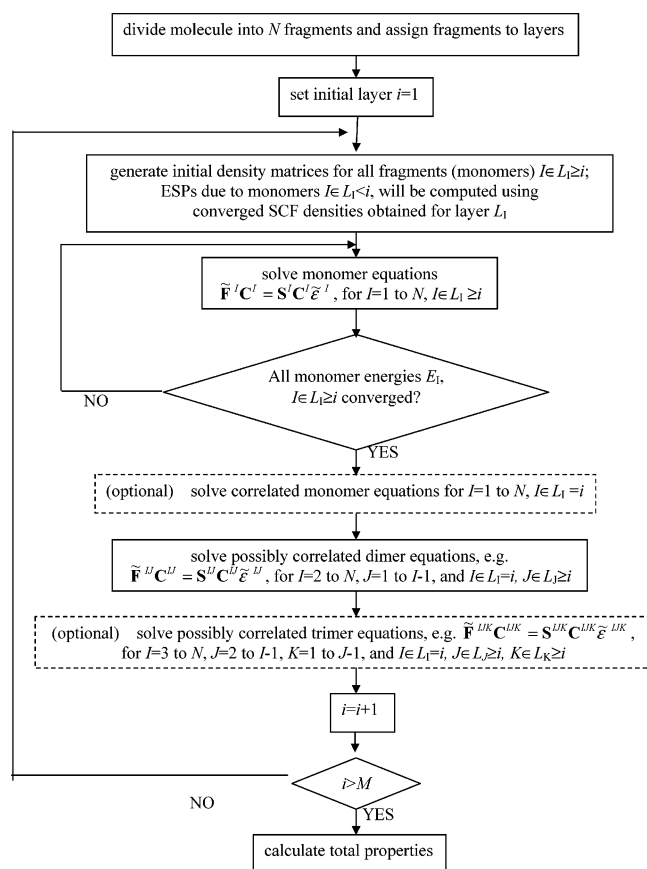
Figure 2. Computational scheme for the multilayer FMO method. L_I denotes the layer to which fragment I belongs. Optional parts shown in dashed rectangles are performed if electron correlation (dynamic correlation, MP2 in this work) or three-body terms are requested.

layers 2 or higher. If necessary, layer 3 calculations follow in the same fashion.

3. Computational Details

3.1. Implementation. The multilayer FMO method was added to the GAMESS program package[12] and parallelized using the generalized distributed data interface (GDDI) developed by Fedorov et al.[13] To achieve reproducible and numerically meaningful data, both atomic and molecular orbital integral accuracy were raised to 10^{-12} using ICUT = 12, ITOL = 24, and CUTOFF = 10^{-12}; SCF convergence was tightened to 10^{-7}; and the same value was used in the monomer SCF cycle where monomer densities converge (that is, monomer SCF calculations are repeated until the maximum difference in monomer energies becomes less than this threshold).

Hybrid sp^3 orbitals of C atom in the projection operators used for the fractioned bonds were obtained from CH_4 calculations as in the previous study.[5] In most of this work bonds were fractioned at sp^3 C atoms, except for the study of fragmentation schemes where some bonds were fractioned at sp^2 carbon atoms as well. In a separate set of tests we verified that using both sp^2- and sp^3-type orbitals for projection operators does not produce any noticeable difference in properties; therefore, sp^3 orbitals were used throughout this work for all calculations.

The following basis sets were used: STO-3G[14],[15] 3-21G,[16] 6-31G, and 6-31G*.[17−19] For d-functions the option to remove s-contaminants (ISPHER = 1) was used. For all DFT studies we employed the B3LYP[20] functional, based on the standard set of the functional parameters in GAMESS and the default grid (96*12*24). In all MP2 calculations the default number of

TABLE 1: Diene and Dienophile Molecules Used in the Diels−Alder Reaction to Evaluate the Accuracy of the Multilayer FMO Method Based on N Fragments[a]

reaction	N	diene	dienophile
A1	3	2-methyl-1,3-butadiene (R_1 is −CH_3)	acrolein (R_2 is −CHO)
A2	3	2-methyl-1,3-butadiene (R_1 is −CH_3)	propene (R_2 is −CH_3)
A3	3	2-methyl-1,3-butadiene (R_1 is −CH_3)	1,4-naphthoquinone (R_3 is −H, R_4 is −H)
A4	4	2-methyl-1,3-butadiene (R_1 is −CH_3)	6-methyl-1,4-naphthoquinone (R_3 is −CH_3, R_4 is −H)
A5	5	2-methyl-1,3-butadiene (R_1 is −CH_3)	6,9-dimethyl-1,4-naphthoquinone (R_3 is −CH_3, R_4 is −CH_3)
B1	3	2-*tert*-butyl-1,3-butadiene (R_1 is −$C(CH_3)_3$)	acrolein (R_2 is −CHO)
B2	3	2-*tert*-butyl-1,3-butadiene (R_1 is −$C(CH_3)_3$)	propene (R_2 is −CH_3)

[a] Structures showing the use of substituents R_1−R_4 are given in Figure 3.

core orbitals was not correlated (that is, 1s orbitals for C and O atoms). The following default approximation thresholds[7] were used for all FMO calculations: RESPAP = 1.0, RESPPC = 2.0, RESDIM = 2.0, and RCORSD = 2.0 (the latter applies only to FMO-MP2).

3.2. Structures and Fragmentation. The Diels−Alder reaction was studied for a few representative sets of dienes and dienophiles summarized in Table 1. Fragmentation information is given in Figure 3 and structures are described in Figure 4 and Table 2. Substituents $R_3 = $ −H (A3, A4) and $R_4 = $ −H (A4) were included in the fragment containing benzene ring. From the possible conformations of the reactants and products we chose the most stable ones, that is, cis for dienes with substituents in the trans position and endo for products. A concertive reaction path was chosen in all cases.

Structures[21] for all molecules and transition states were optimized at the RHF level using the 6-31G* basis set with the default gradient threshold of 10^{-4}. Minima and transition states were verified by computation of analytic second derivatives, and the reaction paths were followed with the intrinsic reaction coordinate (IRC) method. Thus obtained structures were then used for single-point calculations with appropriate ab initio or FMO based methods.

The purpose of this study is to estimate general accuracy and applicability of the two-layer method compared to the one-layer FMO and underlying ab initio methods, rather than comparing to experiment directly. For this particular reaction, MP2 significantly underestimates the reaction barrier and overestimates the reaction heat, while B3LYP produces better results. However, in general both MP2 and DFT methods are of considerable importance with their own advantages and disadvantages so that both are utilized to estimate performance of the multilayer method in this study. For the sake of uniform notation we will refer to regular RHF, B3LYP, and MP2 methods applied to the full system as ab initio, while understanding certain empirical nature of some DFT functionals.

4. Results and Discussion

4.1. Bond Fractioning. For reactions A1, A2, B1, and B2, the total system can be divided into fragments in four different ways, shown in Figure 3, since bonds and molecular orbitals in the FMO method are fractioned at an atom, not between two atoms. The middle fragment is the active site and it is handled at the highest level (layer 2, 6-31G*), whereas for the remaining two fragments (corresponding to substituents) assigned to layer 1, four different basis sets were used. The results are given in

Multilayer Fragment Molecular Orbital Method

J. Phys. Chem. A, Vol. 109, No. 11, 2005 **2641**
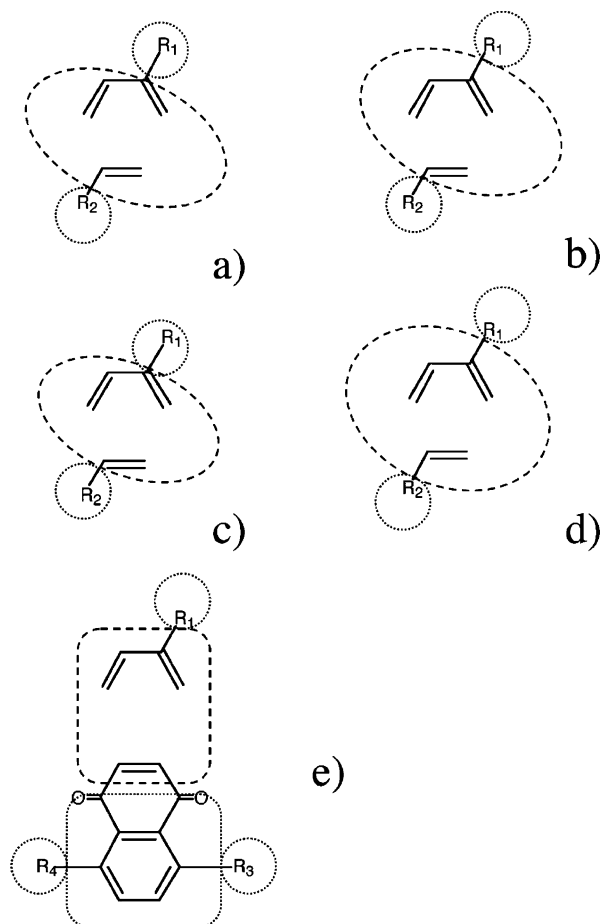
Figure 3. Fragmentation of molecules in the Diels−Alder reaction. The active sites are shown with dashed ellipses and the substituents R_1−R_4 (defined in main text) are shown with dotted circles. The position of circles indicates where bonds are fractioned. Fragmentation schemes S1−S4 tried for reaction A1 are shown in (a) S1, (b) S2, (c) S3, (d) S4. S4 was chosen for all following calculations of reactions A1, A2, B1, and B2. The scheme used for reactions A3−A5 is shown in (e).

Table 3, where the accuracy of the FMO method based on four different fragmentation schemes is compared to the full RHF values (zero point energy correction was not added throughout this work).

As can be seen from Table 3, the single-layer FMO method based on all four schemes reproduces the full RHF properties with at most 1.7 kcal/mol (E_{act}) and 5.7 kcal/mol (E_{form}) error, with S3 scheme giving a particularly bad E_{form} value. S2 and S3 schemes do not show systematic behavior in reproducing the reaction heat and the activation barrier due bond fragmentation between the active site and the substituent R_2, which becomes apparent as the basis set quality in the lower layer decreases. Schemes S1 and S4, on the other hand, show systematic behavior; that is, decrease in the quality of reproducing the ab initio properties as the quality of the lower layer basis set degrades.

The reason for schemes S2 and S3 producing poorer results is the nature of the substituent R_2 that for reaction A1 is −CHO, in which case there is a certain resonance character to the bond that is fractioned. As found by other calculations (not shown) for R_2 equal to −CH$_3$, no such behavior is observed and the quality of results is high for both S2 and S3.

By analyzing schemes S1−S4, we chose scheme S4 as the most accurate and used it for all reactions studied. We note that, with the exception of STO-3G which is too stiff (not
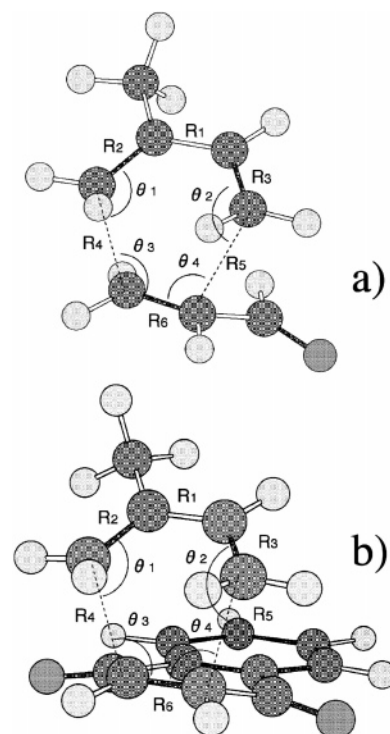
Figure 4. Geometric parameters defining reactant, product and transition state structures for (a) reactions A1, A2, B1, B2, and (b) reactions A3−A5. The structures actually plotted are transition states for reactions (a) A1 and (b) A3.

polarizable), the quality of two-layer results is reasonable for the properties shown. For instance, for the 3-21G basis set the errors in E_{act} and E_{form} relative to one-layer FMO are 3.2 and 2.3 (kcal/mol), respectively.

Based on the results of this study and our experience, we conclude that the best possible location where bonds should be fractioned in the FMO method is at atoms with single bonds, such as sp^3 C. It is particularly bad to fraction bonds at an atom that is involved in electron delocalization, such as bonds in the resonance structures including aromatic rings and other double bond conjugation. If possible, bonds should not be fractioned very close to the active site and a few extra adjacent atoms or groups should be included in the same fragment.

4.2. Mixing Basis Sets. The results of one and two-layer FMO calculations for reactions A1, A2, B1, and B2 in comparison with regular ab initio methods are presented in Table 4, and the fragment assignment to layers is described in section 4.1. The active site was included in the higher layer (i.e., computed with the 6-31G* basis set), whereas smaller basis sets were used for substituents. The only experimental value for comparison we found is the reaction barrier of 18.7 ± 0.8 kcal/mol for reaction A1,[22] which compares favorably to our value (FMO2−B3LYP/6-31G*) of 15.4 kcal/mol given in Table 4.

One-layer FMO2 results agree with ab initio methods within at most (kcal/mol): 1.3 (RHF), 0.7 (B3LYP), and 0.5 (MP2) for E_{act}, and for E_{form} the errors are 0.3 (RHF), 0.1 (B3LYP), and 0.3 (MP2). At all levels (RHF, MP2, B3LYP) the accuracy is better in the case of $R_2 = -$CH$_3$ (reactions A2 and B2). When comparing reactions A1 with B1 and A2 with B2, one can see in general higher accuracy for the B1 and B2 reactions, which comes from larger substituent R_1 ($R_1 = -$CH$_3$ used in A1 and A2 reactions is very small).

The two-layer results are also in satisfactory agreement with full ab initio values, with the exception of the STO-3G basis

TABLE 2: Bond Lengths R in Å and Angles θ in Degrees Defining Reactant (RT), Transition State (TS), and Product (PT) Structures (optimized at the RHF/6-31G* level) for Reactions A1−A5 and B1−B2 (see Figure 4 for notation)

		A1	B1	A2	B2	A3	A4	A5
RT	R_1	1.4880	1.4939	1.4880	1.4939	1.4880	1.4880	1.4880
	R_2	1.3238	1.3250	1.3238	1.3250	1.3238	1.3238	1.3238
	R_3	1.3217	1.3223	1.3217	1.3223	1.3217	1.3217	1.3217
	R_6	1.3210	1.3210	1.3184	1.3184	1.3231	1.3200	1.3161
TS	R_1	1.3976	1.4017	1.3980	1.4019	1.3950	1.3956	1.3958
	R_2	1.3880	1.3900	1.3809	1.3829	1.3866	1.3855	1.3852
	R_3	1.3722	1.3728	1.3764	1.3772	1.3798	1.3797	1.3795
	R_4	2.0712	2.0796	2.1956	2.1903	2.1746	2.1852	2.1881
	R_5	2.3362	2.3238	2.2188	2.2072	2.2144	2.2088	2.1976
	R_6	1.3926	1.3918	1.3851	1.3863	1.3953	1.3919	1.3901
	θ_1	103.79	104.79	104.43	105.22	104.04	104.16	104.58
	θ_2	101.93	102.43	102.07	102.96	103.46	103.62	103.76
	θ_3	111.18	110.72	110.49	110.19	109.11	109.15	109.05
	θ_4	105.62	105.59	106.27	106.22	108.14	108.27	108.57
PT	R_1	1.3222	1.3253	1.3220	1.3252	1.3222	1.3222	1.3214
	R_2	1.5141	1.5215	1.5147	1.5221	1.5129	1.5127	1.5130
	R_3	1.5086	1.5092	1.5093	1.5093	1.5091	1.5091	1.5076
	R_4	1.5383	1.5399	1.5358	1.5383	1.5538	1.5577	1.5555
	R_5	1.5511	1.5474	1.5487	1.5441	1.5431	1.5430	1.5527
	R_6	1.5523	1.5494	1.5512	1.5501	1.5550	1.5469	1.5466
	θ_1	111.23	112.37	110.22	111.46	112.44	113.09	113.04
	θ_2	112.03	111.72	112.79	112.14	109.64	109.33	111.84
	θ_3	113.98	114.23	113.96	114.19	112.69	113.32	113.19
	θ_4	112.48	111.47	112.18	111.08	111.27	110.96	112.63

TABLE 3: Effect of the Fragmentation Scheme upon Activation Barriers E_{act} and the Reaction Heats E_{form} (in kcal/mol at 0 K) for Reaction A1[a]

scheme[b]	basis sets[c]	E_{act}[d]	E_{form}[e]
S1	6-31G*:6-31G*	39.81	−35.67
	6-31G:6-31G*	39.19	−33.95
	3-21G:6-31G*	34.73	−34.92
	STO-3G:6-31G*	49.30	−28.87
S2	6-31G*:6-31G*	38.42	−36.10
	6-31G:6-31G*	39.12	−41.54
	3-21G:6-31G*	36.28	−50.91
	STO-3G:6-31G*	35.48	−16.15
S3	6-31G*:6-31G*	40.62	−30.35
	6-31G:6-31G*	41.96	−34.12
	3-21G:6-31G*	38.47	−40.87
	STO-3G:6-31G*	35.41	−16.45
S4	6-31G*:6-31G*	37.66	−36.08
	6-31G:6-31G*	35.92	−35.69
	3-21G:6-31G*	34.49	−38.37
	STO-3G:6-31G*	50.15	−31.17

[a] Properties are computed with one and two-layer FMO2−RHF (in the former case the two basis sets are identical and in the latter case RHF is used for both layers). *[b]* See main text for the definition of schemes. *[c]* Basis sets are shown for layers 1 and 2 in this order. *[d]* RHF/6-31G* value is 38.94 kcal/mol. *[e]* RHF/6-31G* value is −36.01 kcal/mol.

set which is consistently an unacceptable choice for most practical purposes, at least with this fragmentation scheme without sufficient buffer zone around the active site included into the same fragment. For the two-layer FMO method and the 3-21G basis set in the lower layer, the errors (kcal/mol) in E_{act} relative to one-layer FMO are at most: 3.5 (RHF), 2.9 (B3LYP), 2.9 (MP2), and for E_{form} the errors are 2.3 (RHF), 2.4 (B3LYP), and 2.4 (MP2). On the other hand, for the 6-31G basis set in the lower layer, the errors (kcal/mol) in E_{act} relative to one-layer FMO are at most 1.7 (RHF), 1.2 (B3LYP), 1.6 (MP2), and for E_{form} the errors are 0.9 (RHF), 1.4 (B3LYP), and 0.4 (MP2). Certainly, if for a given reaction the reaction barrier is a few kcal/mol, care should be taken to choose an appropriately high quality basis set for the lower layer.

4.3. Mixing the Electron Correlation Level. The results of one and two-layer FMO calculations for reactions A1, A2, B1,

and B2 in comparison with regular ab initio methods are summarized in Table 5 for the entries with the same basis set (6-31G*) but different electron correlation level. The active site was included in the higher layer (i.e., computed with electron correlation included), whereas the lower layer was done at the RHF level (with one exception, where we tried MP2 for the higher layer and DFT for the lower).

The two-layer FMO errors in E_{act} compared to one-layer results were found to be at most 5.6 kcal/mol (B3LYP) and 3.4 kcal/mol (MP2), and the errors in E_{form} were 4.6 (B3LYP) and 3.4 (MP2). Larger errors are observed for DFT since MP2 does not change the orbitals and, in addition, DFT has the tendency of producing a smaller HOMO−LUMO gap, thus in case of DFT the effect of environment (lower layer) is stronger.

Performance of the hybrid electron correlation method (B3LYP and MP2) is difficult to estimate by comparing to regular methods. Not fully unexpectedly, it produces results somewhere between pure MP2 and B3LYP. The question of its usefulness is left to future applications when comparison with experiment will perhaps provide a measure of its merits. It is conceivable that physical considerations may dictate describing certain parts of the system with MP2, which has an advantage of good treatment of dispersion interaction, whereas better quality of DFT for reaction heats and other properties may be employed for the active site and other relevant parts of a molecule.

By comparing reactions A1 and B1, as well as A2 and B2, one can deduce that the effect of adding the bulky substituent (*tert*-butyl for reactions B1 and B2) to the diene insignificantly (<0.3 kcal/mol) changes the reaction barrier at both B3LYP and FMO2−B3LYP levels and lowers the reaction heat by about 2 kcal/mol for both B3LYP and FMO2−B3LYP. By comparing structures, the effect of the bulky substituent can be seen from Table 2 to be sterical.

By comparing reactions A1 and A2, as well as B1 and B2, one can deduce that the effect of going from the carbonyl (A1, B1) to methyl (A2, B2) substituent in the dienophile dramatically increases the reaction barrier by 6.9 (A1→A2) and 6.7 (B1→B2) kcal/mol at the regular B3LYP level, whereas for FMO2−B3LYP the corresponding increase is 7.5 and

Multilayer Fragment Molecular Orbital Method

J. Phys. Chem. A, Vol. 109, No. 11, 2005 **2643**

TABLE 4: Activation Barriers E_{act} and the Reaction Heats E_{form} (in kcal/mol at 0 K) for Reactions A1, A2, B1 and B2, Illustrating Basis Set Mixing[a]

method	basis sets[b]	A1		B1		A2		B2	
		E_{act}	E_{form}	E_{act}	E_{form}	E_{act}	E_{form}	E_{act}	E_{form}
RHF	6-31G*	38.94	−36.01	38.88	−33.97	45.77	−37.71	45.61	−35.41
FMO2−RHF:RHF	6-31G*:6-31G*	37.66	−36.08	38.40	−33.99	45.50	−37.76	45.65	−35.42
	6-31G:6-31G*	35.92	−35.69	37.10	−33.08	45.14	−38.09	45.61	−35.16
	3-21G:6-31G*	34.49	−38.37	34.95	−35.91	44.71	−39.37	44.73	−36.48
	STO-3G:6-31G*	50.15	−31.17	48.60	−31.13	48.08	−34.86	46.89	−34.74
B3LYP	6-31G*	15.39	−36.23	15.29	−34.14	22.26	−38.38	21.95	−36.30
FMO2−B3LYP:B3LYP	6-31G*:6-31G*	14.67	−36.32	14.98	−34.17	22.15	−38.46	21.97	−36.30
	6-31G:6-31G*	13.43	−35.30	13.99	−32.80	21.87	−38.88	21.86	−36.31
	3-21G:6-31G*	12.09	−38.79	12.07	−36.58	21.44	−40.68	20.93	−38.23
	STO-3G:6-31G*	24.12	−34.44	23.02	−34.20	24.05	−38.68	23.03	−38.48
MP2	6-31G*	7.38	−48.99	6.16	−47.43	13.91	−50.76	12.48	−49.07
FMO2-MP2:MP2	6-31G*:6-31G*	6.89	−49.26	5.96	−47.63	13.91	−50.84	12.67	−49.07
	6-31G:6-31G*	5.25	−49.29	4.69	−47.42	13.44	−51.27	12.45	−49.23
	3-21G:6-31G*	4.09	−51.65	3.07	−49.96	13.24	−52.33	11.98	−50.34
	STO-3G:6-31G*	19.66	−42.31	17.99	−42.50	17.80	−46.13	16.41	−46.28

[a] Properties are computed with one- and two-layer FMO2 methods (in the former case the two basis sets are identical) as well as ab initio methods. The electron correlation level is the same in both layers for the FMO methods. [b] For FMO methods the basis sets are shown for layers 1 and 2 in this order, otherwise only one basis set is shown.

TABLE 5: Activation Barriers E_{act} and the Reaction Heats E_{form} (in kcal/mol at 0 K) for Reactions A1, A2, B1, and B2, Illustrating Both Basis Set and Electron Correlation Mixing[a]

methods[b]	basis sets[c]	A1		B1		A2		B2	
		E_{act}	E_{form}	E_{act}	E_{form}	E_{act}	E_{form}	E_{act}	E_{form}
RHF	6-31G*	38.94	−36.01	38.88	−33.97	45.77	−37.71	45.61	−35.41
B3LYP	6-31G*	15.39	−36.23	15.29	−34.14	22.26	−38.38	21.95	−36.30
MP2	6-31G*	7.38	−48.99	6.16	−47.43	13.91	−50.76	12.48	−49.07
FMO2−RHF:RHF	6-31G*:6-31G*	37.66	−36.08	38.40	−33.99	45.50	−37.76	45.65	−35.42
FMO2−B3LYP:B3LYP	6-31G*:6-31G*	14.67	−36.32	14.98	−34.17	22.15	−38.46	21.97	−36.30
FMO2-MP2:MP2	6-31G*:6-31G*	6.89	−49.26	5.96	−47.63	13.91	−50.84	12.67	−49.07
FMO2−B3LYP:MP2	6-31G*:6-31G*	12.56	−41.47	12.55	−39.81	18.83	−44.48	18.59	−42.77
FMO2−RHF:B3LYP	6-31G*:6-31G*	9.10	−40.97	10.57	−38.71	19.08	−42.60	19.36	−40.21
	6-31G:6-31G*	7.35	−40.54	9.27	−37.75	18.68	−42.91	19.29	−39.93
	3-21G:6-31G*	5.92	−43.21	7.15	−40.58	18.26	−44.22	18.44	−41.28
	STO-3G:6-31G*	21.37	−35.97	20.58	−35.79	21.55	−39.74	20.56	−39.58
FMO2−RHF:MP2	6-31G*:6-31G*	7.09	−45.97	8.19	−44.20	15.82	−48.50	16.03	−46.52
	6-31G:6-31G*	5.35	−45.56	6.86	−43.25	15.39	−48.90	15.94	−46.33
	3-21G:6-31G*	3.94	−48.27	4.74	−46.11	15.00	−50.14	15.12	−47.60
	STO-3G:6-31G*	19.34	−41.35	18.27	−41.58	18.27	−45.71	17.25	−45.90

[a] Properties are computed with one- and two-layer FMO2 methods (in the former case the two basis sets and methods are identical) as well as ab initio methods. [b] FMO methods are shown for layers 1 and 2 in this order, for full calculations only one method is shown. [c] For FMO methods the basis sets are shown for layers 1 and 2 in this order, otherwise only one basis set is shown.

7.0 (kcal/mol). On the other hand, the reaction heat is increased by 2.2 (A1→A2) and 2.2 (B1→B2) kcal/mol at the regular B3LYP level, whereas for FMO2−B3LYP the corresponding increase is 2.1 and 2.1 (kcal/mol). The effect of the dienophile substituent can be seen from Table 2 to be electronic: the transition state structure parameter R_4 is lengthened and R_5 is shortened (A1→A2 or B1→B2). In other words, methyl substituent destabilizes the transition state (compared to carbonyl) by acting as electron donor.

4.4. Mixing Both Basis Sets and the Electron Correlation Level. The results of one- and two-layer FMO calculations for reactions A1, A2, B1, and B2 in comparison with regular ab initio methods are summarized in Table 5. The active site was included in the higher layer (i.e., computed with electron correlation included and better basis set), whereas the lower layer was done at the RHF level and a smaller basis set.

The general trends follow previously described trends for separate mixing of basis sets and electron correlation. As the basis set describing the environment becomes smaller, the error becomes larger. For instance, for the two-layer FMO method and the 3-21G basis set in the lower layer, the errors (kcal/mol) in E_{act} relative to one-layer FMO are at most

8.7 (B3LYP), 3.0 (MP2), and for E_{form} the errors are 6.9 (B3LYP) and 1.5 (MP2). On the other hand, for the 6-31G basis set in the lower layer the errors (kcal/mol) in E_{act} relative to one-layer FMO are at most 1.8 (B3LYP), 1.7 (MP2), and for E_{form} the errors are 1.0 (B3LYP) and 1.0 (MP2).

B3LYP results indicate stronger effects of the environment and higher demand for the basis set quality. In practical applications it may be necessary to employ three-layer calculations with an intermediate layer included.

4.5. Accuracy Dependence upon the Number of Fragments. The results of one and two-layer FMO calculations for reaction A3, A4, and A5 in comparison with regular ab initio methods are presented in Table 6, and the fragment assignment to layers is illustrated in Figure 3. The active site was included in the higher layer (i.e., computed with the 6-31G* basis set), whereas smaller basis sets were used for substituents.

One-layer FMO2 results agree with ab initio methods within at most (kcal/mol) 1.2 (RHF), 0.8 (B3LYP), and 0.5 (MP2) for E_{act}, whereas for E_{form} the errors are 1.5 (RHF), 1.9 (B3LYP), and 2.0 (MP2). For the two-layer FMO method using the 3-21G basis set in the lower layer, the errors (kcal/mol) in E_{act} relative to one-layer FMO are at most 5.5 (RHF), 3.0 (B3LYP),

TABLE 6: Activation Barriers E_{act} and the Reaction Heats E_{form} (both in kcal/mol at 0 K) for Reactions A3, A4, and A5, Illustrating the Accuracy Dependence upon the Number of Fragments[a]

method	basis sets[b]	A3		A4		A5	
		E_{act}	E_{form}	E_{act}	E_{form}	E_{act}	E_{form}
RHF	6-31G*	37.72	−30.27	35.40	−31.80	31.85	−36.05
FMO2−RHF:RHF	6-31G*:6-31G*	38.87	−30.55	36.13	−32.21	31.81	−37.52
	6-31G:6-31G*	37.90	−31.99	35.85	−32.95	32.48	−36.05
	3-21G:6-31G*	33.41	−34.91	32.76	−35.32	31.04	−35.95
	STO-3G:6-31G*	60.04	−22.52	57.01	−23.93	52.15	−29.11
B3LYP	6-31G*	15.13	−30.24	13.35	−31.55	10.60	−34.51
FMO2−B3LYP:B3LYP	6-31G*:6-31G*	15.50	−30.74	13.27	−32.01	9.77	−36.39
	6-31G:6-31G*	15.45	−31.55	13.74	−32.50	11.22	−33.94
	3-21G:6-31G*	12.49	−35.07	12.34	−35.44	11.58	−34.11
	STO-3G:6-31G*	34.77	−27.28	33.33	−27.81	30.72	−29.30
MP2	6-31G*	0.00	−47.25	−2.75	−49.23	−7.44	−54.73
FMO2-MP2:MP2	6-31G*:6-31G*	0.51	−48.39	−2.64	−50.47	−7.83	−56.75
	6-31G:6-31G*	0.53	−50.24	−2.09	−51.71	−6.62	−56.06
	3-21G:6-31G*	−1.83	−52.26	−2.49	−52.79	−4.86	−53.22
	STO-3G:6-31G*	27.59	−34.94	25.17	−35.94	20.92	−39.12

[a] Properties are computed with one- and two-layer FMO2 methods (in the former case the two basis sets are identical) as well as ab initio methods. [b] For FMO methods the basis sets are shown for layers 1 and 2 in this order, otherwise only one basis set is shown.

3.0 (MP2), and for E_{form} the errors are 4.4 (RHF), 4.3 (B3LYP), and 3.9 (MP2). On the other hand, for the 6-31G basis set in the lower layer the errors (kcal/mol) in E_{act} relative to one-layer FMO are at most 1.0 (RHF), 2.4(B3LYP), 1.2 (MP2), and for E_{form} the errors are 1.5 (RHF), 2.4 (B3LYP), and 2.0 (MP2). We note that MP2 predicts too low barriers for the Diels−Alder reaction (in fact, no barrier for reactions A3−A5 based on RHF structures).

Adding methyl substituents in 6 and in 6,9 positions significantly lowers the reaction barrier by 1.8 (2.3) and 4.5 (5.9) kcal/mol at the regular B3LYP (the values for RHF are in parentheses) level, respectively, and increases the reaction heat by 1.3 (1.5) and 4.3 (5.8) kcal/mol at the regular B3LYP (the values for RHF are in parentheses) level, respectively. The FMO method follows this trend, e.g., for the one-layer case the corresponding lowering is 1.8 (2.7) and 5.7 (7.0) and the corresponding increase is 1.3 (1.7) and 5.6 (7.0). The effect of adding methyl substituents to diene can be seen from Table 2 to be mostly electronic: the transition state structure parameter R_4 is somewhat lengthened and R_5 is somewhat shortened, stabilizing the transition state.

There appears to be no distinct tendency for the errors to grow with the number of fragments for the systems studied in this work, although in a few cases the errors are larger for the largest system. We note that the general quality of the three-body FMO method has been established[5] to be within chemical accuracy (1 kcal/mol), provided that the fragments are sufficiently large (such as two residues per fragment for polypeptides). The small size of molecules in the Diels−Alder reaction forced us to use small fragment size and the two-body expansion (the three-body FMO method exactly converges to the full ab initio results if three fragments are present); however, in practical applications sufficient accuracy should be achieved with properly chosen fragmentation.

4.6. Benchmark Calculations. Cyclodextrins (CD, that is, α, β, and γ cyclic oligomers of α-D-glucose containing 6, 7, and 8 subunits, respectively) have attracted much attention in the field of supramolecular chemistry.[23−25] Owing to the nonpolar macrocyclic cavity inside its structure, cyclodextrins can form inclusion compounds with variety of polar and nonpolar organic guest molecules. Also, cyclodextrins are known to accelerate some chemical reactions, such as the decarboxylation of phenylcyanoacetate anion (PCAA) and the hydrolysis of phenolic esters. Because of computational limitations,

most of the earlier theoretical calculations of cyclodextrin-catalyzed chemical reactions were based on the empirical valence bond (EVB) or semiempirical approaches.[26−29]

To demonstrate the computational efficiency of the multilayer FMO method, we evaluate the gas-phase activation energy of the decarboxylation of PCAA catalyzed by β-CD. The structure was obtained from a quantum mechanics/molecular mechanics (QM/MM)[30,31] study by Ishida[32] where PCAA was treated as the QM region (RHF/6-31G*) and β-CD as the MM region (MM2 force field[33]). The reaction coordinate was chosen to be the C−COO bond distance, and the reaction path including the transition state was obtained by performing full geometry optimizations with the reaction coordinate fixed.

In the FMO calculations, each α-D-glucose and PCAA were treated as one fragment, with eight fragments total. In the two-layer calculations only PCAA was assigned to the second (higher) layer. The 3-21(+)G and 6-31(+)G* basis sets were used, where (+) indicates that diffuse functions were added to the COO− functional group in PCAA. The number of atoms was 165 and the number of atomic orbitals was 965 and 1499 for 3-21(+)G and 6-31(+)G*, respectively. The results are presented in Table 7, where the errors in the activation energy and timings on a 16 node 3.0 GHz Pentium4 cluster are given.

The computational cost of multilayer FMO is approximately additive, given by the sum of costs for each layer (based on the number of fragments, the wave function type, and the basis set in the layer). In addition, usually a much smaller amount of extra work was spent on computing interlayer ES potentials from lower layer fragments. The scaling of the unilayer FMO method was discussed in refs 34, 7, and 8 for FMO2−RHF, FMO2-MP2, and FMO2-MCSCF, respectively. In the latter two cases the computational scaling with system size was found to be nearly linear.

One can see from Table 7 that the unilayer FMO results are in good agreement with full ab initio values, the RHF errors being −1.15, −2.19 for 3-21(+)G and 6-31(+)G*, respectively, and the DFT errors being −1.31 and −2.62 (in kcal/mol, relative to the same basis set ab initio method). It is also clear that the activation barrier for 3-21(+)G basis set is significantly overestimated (8.53 and 7.12 kcal/mol for RHF and DFT, respectively, at the ab initio level). The two-layer FMO method has the errors of −1.94 and −2.12 kcal/mol for RHF and DFT, respectively, when only the basis set changes between the two layers. The error becomes 3.04 kcal/mol when only the wave

Multilayer Fragment Molecular Orbital Method

J. Phys. Chem. A, Vol. 109, No. 11, 2005 **2645**

TABLE 7: Benchmark Calculations of the Activation Barrier (E_{act} at 0 K) for the Gas-Phase Decarboxylation of PCAA Catalyzed by β-CD[a]

method	ΔE_{act}	T
RHF/6−31(+)G*	0.00[b]	13141.4
RHF/3-21(+)G	8.53[b]	2462.1
FMO2−RHF/6−31(+)G*	−1.15[b]	9610.5
FMO2−RHF/3-21(+)G	6.34[b]	1274.2
FMO2−RHF/3-21(+)G:RHF/6−31(+)G*	−1.94[b]	1370.8
DFT/6−31(+)G*	0.00[c]	55058.9
DFT/3-21(+)G	7.12[c]	23129.6
FMO2-DFT/6−31(+)G*	−1.31[c]	31767.0
FMO2-DFT/3-21(+)G	4.50[c]	11743.3
FMO2-DFT/3-21(+)G:DFT/6−31(+)G*	−2.12[c]	11892.4
FMO2−RHF/6−31(+)G*:DFT/6−31(+)G*	3.04[c]	10117.4
FMO2−RHF/3-21(+)G:DFT/6−31(+)G*	1.04[c]	1527.4

[a] The error ΔE_{act} relative to the reference is shown in kcal/mol and the timings T on a 16 node 3.0 GHz Pentium4 cluster connected by Gigabit Ethernet are given in seconds (for two single-point gradient calculations of the reactant complex and the transition state). [b] Relative to the reference $E_{act} = 25.6$ kcal/mol for RHF/6−31(+)G*. [c] Relative to the reference $E_{act} = 16.8$ kcal/mol for DFT/6−31(+)G*.

function type is varied, and it is 1.04 kcal/mol when both the wave function type and the basis set differ between the layers. We note that the values of errors are of a very similar magnitude compared with much smaller systems in the Diels−Alder reaction covered above, thus, at least in the cases considered, the errors do not grow noticeably with system size.

The FMO method was faster than ab initio in all cases. For the system considered, the two-layer FMO method without wave function type mixing was found to be 9.6 and 4.6 times faster than the regular RHF and DFT methods, respectively. When both the wave function type and the basis set were mixed, the two-layer FMO method (FMO2−RHF/3-21(+)G:DFT/6-31(+)G*) was 36 times faster than the regular DFT while the error was only 1.04 kcal/mol.

5. Conclusions

The fragmentation scheme study demonstrated weak dependence of properties upon the fragmentation position, and general guidelines for the optimum way to divide molecules into fragments were established (that is, if possible, bonds should be fractioned at sp³ atoms). The one-layer FMO error in the activation barriers and reaction heats for the Diels−Alder reaction was 2.0 kcal/mol or less for all levels applied (RHF, B3LYP, and MP2), relative to the full ab initio methods, which demonstrated sufficient accuracy and validated application of the FMO methods to studies of chemical reactions. Excellent reproduction of reaction barrier and heat trends due to diene and dienophile substituents was established for the one-layer FMO method compared to the full ab initio properties.

The multilayer FMO method proposed in this work has been applied to the Diels−Alder reaction with various basis sets and electron correlation levels assigned to layers. It was found that for the given system the STO-3G basis set used for substituents does not deliver acceptable accuracy. Using lower electron correlation levels or smaller basis sets for substituents was found to give a somewhat larger error of several kcal/mol, indicating the need in practical applications for larger systems, either to enlarge the active site or to include fragments adjacent to the active site into the same higher layer. DFT-based two-layer FMO methods were observed to have somewhat larger errors compared to RHF and MP2, which is attributed to electron correlation, which for DFT is taken into account self-consistently. It was also shown that increasing the number of

fragments does not noticeably decrease the accuracy of results for the reaction used in this study.

For the large majority of cases, somewhat larger errors in activation barriers compared to reactions heats were observed. This is taken to indicate a stronger effect of environment (substituents) upon the transition state.

Benchmark calculations of activation energies for the system with 165 atoms demonstrated that the errors relative to ab initio methods are of the same magnitude as for the much smaller case of Diels−Alder reactions and, second, that the two-layer method is highly computationally efficient, being 36 times faster than the regular DFT (for the case of mixing both the basis set and the wave function type).

Multilayer formalism will be extended in the future to include molecular mechanics when an appropriate formulation linking the FMO method and molecular mechanics is proposed. It should be noted that high accuracy[5] and high parallel efficiency[13] of the FMO method permits quantum mechanical calculations of rather larger systems (an all-electron calculation of a molecule containing 4000 atoms has been reported[35]), thus the need for molecular mechanics is not as stringent as for other methods.

Supporting Information Available: A representative set of GAMESS input files containing geometry and fragmentation information. This material is available free of charge via the Internet at http://pubs.acs.org.

References and Notes

(1) Kitaura, K.; Ikeo, E.; Asada, T.; Nakano, T.; Uebayasi, M. *Chem. Phys. Lett.* **1999**, *313*, 701.
(2) Kitaura, K.; Sugiki, S.-I.; Nakano, T.; Komeiji, Y.; Uebayasi, M. *Chem. Phys. Lett.* **2001**, *336*, 163.
(3) Nakano, T.; Kaminuma, T.; Sato, T.; Fukuzawa, K.; Akiyama, Y.; Uebayasi, M.; Kitaura, K. *Chem. Phys. Lett.* **2002**, *351*, 475.
(4) Komeiji, Y.; Nakano, T.; Fukuzawa, K.; Ueno, Y.; Inadomi, Y.; Nemoto, T.; Uebayasi, M.; Fedorov, D. G.; Kitaura, K. *Chem. Phys. Lett.* **2003**, *372*, 342.
(5) Fedorov, D. G.; Kitaura, K. *J. Chem. Phys.* **2004**, *120*, 6832.
(6) Fedorov, D. G.; Kitaura, K. *Chem. Phys. Lett.* **2004**, *389*, 129.
(7) Fedorov, D. G.; Kitaura, K. *J. Chem. Phys.* **2004**, *121*, 2483.
(8) Fedorov, D. G.; Kitaura, K. *J. Chem. Phys.* **2005**, *122*, 054108.
(9) Svensson, M.; Humbel, S.; Froese, R. J.; Matsubara, T.; Sieber, S.; Morokuma, K. *J. Phys. Chem.* **1996**, *100*, 19357.
(10) Houk, K. N.; Li, Y.; Evanseck, J. D. *Angew. Chem., Int. Ed. Engl.* **1992**, *31*, 682.
(11) Houk, K. N.; Gonzalez, J.; Li, Y. *Acc. Chem. Res.* **1995**, *28*, 81.
(12) Schmidt, M. W.; Baldridge, K. K.; Boatz, J. A.; Elbert, S. T. Gordon, M. S.; Jensen, J. H.; Koseki, S.; Matsunaga, N.; Nguyen, K. A.; Su, S.; Windus, T. L.; Dupuis, M.; Montgomery, J. A. Jr. *J. Comput. Chem.* **1993**, *14*, 1347.
(13) Fedorov, D. G.; Olson, R. M.; Kitaura, K.; Gordon, M. S.; Koseki, S. *J. Comput. Chem.* **2004**, *25*, 872.
(14) Hehre, W. J.; Stewart, R. F.; Pople, J. A. *J. Chem. Phys.* **1969**, *51*, 2657.
(15) Hehre, W. J.; Ditchfield, R.; Stewart, R. F.; Pople, J. A. *J. Chem. Phys.* **1970**, *52*, 2769.
(16) Binkley, J. S.; Pople, J. A.; Hehre, W. J. *J. Am. Chem. Soc.* **1980**, *102*, 939.
(17) Ditchfield, R.; Hehre, W. J.; Pople, J. A. *J. Chem. Phys.* **1971**, *54*, 724.
(18) Hehre, W. J.; Ditchfield, R.; Pople, J. A. *J. Chem. Phys.* **1972**, *56*, 2257.
(19) Hariharan, P. C.; Pople, J. A. *Theor. Chim. Acta* **1973**, *28*, 213.
(20) Hertwig, H.; Koch, W. *Chem. Phys. Lett.* **1997**, *268*, 345.
(21) Complete structures along with fragmentation information can be downloaded from: http://staff.aist.go.jp/d.g.fedorov/fmo/data.html.
(22) Kistiakowsky, G. B.; Lacher, J. R. *J. Am. Chem. Soc.* **1936**, *58*, 123.

Fedorov et al.

(23) Bender, M. L.; Komiyama, M. *Cyclodextrin Chemistry*; Springer: Berlin, 1978.

(24) Lehn, J. M. *Supramolecular Chemistry*; VCH: Weinheim, 1978.

(25) *Chem. Rev.*, special cyclodextrin issue, **1998**, *98*.

(26) Luzhkov, V. B.; Venanzi, C. A. *J. Phys. Chem.* **1995**, *99*, 2312.

(27) Lipkowitz, K. B. *Chem. Rev.* **1998**, *98*, 1829.

(28) Luzhkov, V.; Åqvist, J. *J. Am. Chem. Soc.* **1998**, *120*, 6131.

(29) Furuki, T.; Hosokawa, F.; Sakurai, M.; Inoue, Y.; Chyujo, R. *J. Am. Chem. Soc.* **1993**, *115*, 2903.

(30) Ishida, T.; Kato, S. *J. Am. Chem. Soc.* **2003**, *125*, 12035.

(31) Ishida, T.; Kato, S. *J. Am. Chem. Soc.* **2004**, *126*, 7111.

(32) Ishida, T., in preparation.

(33) Burkert, U.; Allinger, N. L. *Molecular Mechanics*; American Chemical Society: Washington, D. C., 1982.

(34) Ishimoto, T.; Tokiwa, H.; Teramae, H.; Nagashima, U. *Chem. Phys. Lett.* **2004**, *387*, 460.

(35) Fukuzawa, K.; Kitaura, K.; Uebayasi, M.; Nakata, K.; Kaminuma, T.; Nakano, T. *J. Comput. Chem.* **2005**, *26*, 1.